Electronic Structures and Chemical Bonding of Fluorinated Fullerenes Studied by NEXAFS, UPS, and Vacuum-UV Absorption Spectroscopies

Ryuichi Mitsumoto, Tohru Araki, Eisuke Ito, Yukio Ouchi, and Kazuhiko Seki*

Department of Chemistry, Faculty of Science, Nagoya University, Chikusa-ku, Nagoya 464-01, Japan

Koichi Kikuchi and Yohji Achiba

Department of Chemistry, Faculty of Science, Tokyo Metropolitan University, Hachioji 192-03, Japan

Hiroshi Kurosaki, Takaaki Sonoda, and Hiroshi Kobayashi

Institute of Advanced Material Study, Kyushu University, Kasuga 816, Japan

Olga V. Boltalina, Valeria K. Pavlovich, and Lev N. Sidorov

Chemistry Department, Moscow State University, Moscow, 119899, Russia

Yoshiyuki Hattori, Ning Liu, Sumitoshi Yajima, Shinji Kawasaki, Fujio Okino, and Hidekazu Touhara

Department of Chemistry, Faculty of Textile Science and Technology, Shinshu University, Ueda 386, Japan

Received: September 3, 1997; In Final Form: November 10, 1997[⊗]

The chemical bonding and the electronic structures of $C_{60}F_x$ and $C_{70}F_x$ were investigated by near edge X-ray absorption fine structure (NEXAFS) spectroscopy and UV photoemission spectroscopy (UPS), which are useful methods for examining the unoccupied and the occupied states, respectively. With these results and XPS measurements, we derived the electronic energy diagram of $C_{60}F_x$ and discussed the change of the electronic structure from that of C_{60} by fluorination. The energies of the LUMO and the Fermi level of solid $C_{60}F_{48}$ were estimated to be −5.0 and −5.4 eV below the vacuum level, indicating that highly doped $C_{60}F_x$ is a strong electron acceptor. The electronic absorption spectra of $C_{60}F_x$ solutions deep into the vacuum-ultraviolet region were also measured, and the isomerism of $C_{60}F_x$ was discussed by comparing the observed results with theoretical simulations.

I. Introduction

Since the discovery of C_{60} in 1985,[1] fluorinated fullerenes such as $C_{60}F_x$ form a class of attractive compounds with potential applications such as cathode materials of a high energy density battery.[2−4] Recent electrochemical studies[4] showed that the open-circuit voltage of $C_{60}F_x$ is higher than that of C_{60} by about 1 V. This indicates that the electronic structure of C_{60} is significantly changed by fluorination. For further understanding of such performance and other applications to electric and electronic devices, information on the electronic structure is essential.

There have been several studies of the electronic structure of fluorinated fullerenes by using UV photoemission spectroscopy (UPS),[5] electron affinity estimation in gas-phase reaction,[6] and UV−visible absorption spectroscopy.[7,8] As for the core level electronic structure, X-ray photoelectron spectroscopy (XPS) measurements[9,10] have been performed. Although these reports have offered important information, our understanding about the electronic structures of fluorinated fullerenes is still insufficient. For example, there has been no report of the work function of the fluorinated fullerenes.

Also, there have been few studies about the effect of the distribution of the degree of fluorination and the coexistence of geometrical isomers. Fluorination under usual conditions has been reported to result in the mixture of various compounds with different fluorine number x.[11] Recently, there have been two reports about the preparation of the fluorinated fullerene with a unique x. Gakh et al.[12] have selectively prepared $C_{60}F_{48}$ and proposed its symmetry from ^{19}F NMR measurements. Boltalina et al.[13] have also found new selective preparation methods of $C_{60}F_{36}$. However, even the $C_{60}F_x$ molecule with a unique x may have several geometrical isomers as indicated by the theoretical calculations for $C_{60}H_{36}$.[14−16]

In this paper, we report the investigations of the chemical bonding and the electronic structures of fluorinated fullerenes, $C_{60}F_x$ and $C_{70}F_x$, by near edge X-ray absorption fine structure (NEXAFS) spectroscopy[17] and UPS, which are useful methods for examining the unoccupied and the occupied valence states, respectively. NEXAFS study also offers information about chemical bonding. With these results and the XPS measurements, we derived a comprehensive energy diagram for $C_{60}F_x$ covering the wide energy range from the core to the unoccupied levels and discussed the correlation of the electronic structures with those of C_{60}. Similar results were obtained for $C_{70}F_x$. For $C_{60}F_x$, the dependence of the electronic structure on x was also examined.

[⊗] Abstract published in *Advance ACS Abstracts,* December 15, 1997.

S1089-5639(97)02863-6 CCC: $15.00
Published on Web 01/15/1998

We also measured the electronic absorption spectra of $C_{60}F_{36}$ and $C_{60}F_{42}$ in solution, deep into the vacuum-ultraviolet (VUV) region. By the comparison with theoretically simulated spectra for four probable isomers of $C_{60}F_{36}$, we examined whether it is possible to predict the symmetry of $C_{60}F_x$.

II. Experimental and Theoretical Section

The C_{60} powder for fluorination was mostly prepared by the usual arc-discharge method and chromatographic technique.[18] Some part of C_{60} and the whole C_{70} material were supplied from Vacuum Metallurgical Co. Ltd. The NEXAFS and the UPS measurements were performed for fluorinated C_{60} and C_{70}, while the VUV absorption measurements were carried out only for fluorinated C_{60} samples. The samples for the NEXAFS and the UPS measurements were prepared as thin films by vacuum evaporation on Ni substrates, which is resistant to the corrosion by fluorine. Ag substrates were also used in some cases. Fluorinated fullerenes were prepared by the reaction of fullerenes with fluorine gas of atmospheric pressure in two ways. In one method, fullerene powder was reacted with F_2 gas, and the fluorinated powder was evaporated. In the other method, fullerene powder was evaporated to form a thin film, and the film was reacted with F_2 gas. The samples prepared in these two ways showed qualitatively similar results. The evaporation was performed under vacuum of 10^{-5} Torr. The thickness of the films was monitored with a quartz oscillator during the evaporation and was adjusted to be 7−200 nm. The thicknesses of around 10 and 100 nm were adopted for UPS and NEXAFS measurements, respectively.

The degrees of fluorination could be adjusted by the reaction conditions, i.e., the reaction time and temperature. The fluorine content x of the sample, defined as the number of fluorine atoms per fullerene molecule, was varied from 11 to 48 by the reaction with 1 atm of F_2 gas at 20−200 °C for 3 min−14 days. We also prepared $C_{60}F_{36}$ with unique x by using the reaction of C_{60} with MnF_3 at 330 °C for 24 h. This preparation method was reported in detail elsewhere.[13] The fluorine contents were estimated by XPS measurements. For the samples prepared by the evaporation of fluorinated fullerenes, we carried out XPS measurements before and after evaporation. These results showed that the fluorine content was little changed by the vacuum evaporation.

NEXAFS measurements were performed at the beamline 11A of the Photon Factory at National Laboratory for High Energy Physics (KEK-PF) at Tsukuba, by using synchrotron radiation monochromatized by a Grasshopper monochromator with a grating of 2400 lines/mm. The spectra were obtained in the total electron yield mode. The resolution was estimated to be 0.3 and 0.7 eV at the C and F K-edges, respectively. Energy calibration was performed by referring to the spectra of hexatriacontane (n-$C_{36}H_{78}$) for the C K-edge and tetrafluoroethylene oligomer for the F K-edge as the second standard. The spectra of these compounds have been calibrated by using various vapor spectra.[19] Energy calibration for the C K-edge was also performed by assuming the two dips in the photon intensity distribution by carbon contamination on the optical components to be 284.7 and 291.0 eV.[20] All the presently measured NEXAFS spectra show little dependence on the incidence angle of light, indicating that these fluorinated fullerene molecules had no significantly preferable molecular orientation.

UPS measurements were performed by using two experimental setups, i.e., (1) the beamline 8B2 of UVSOR facility at Institute for Molecular Science (IMS) at Okazaki, by using synchrotron radiation monochromatized by a plane grating monochromator[21] and an electrostatic deflector-type analyzer, and (2) a conventional laboratory system by using a discharge lamp capable of the He I (21.2 eV) and Ar I (11.7 eV) resonance lines and a retarding field-type analyzer. The resolution was estimated to be about 0.2 eV for both cases. The work function of the samples was estimated under the assumption that the Fermi levels of these fluorinated fullerenes align with that of the substrate. The contact potential difference with the collector of the retarding field-type energy analyzer was measured from the low energy cutoff of the spectra, and the work function was deduced from the separately determined work function of the collector.

The solution samples for the VUV absorption measurements were prepared by using perfluoromethylcyclohexane (C_7F_{14}) as the solvent. Since this solvent is prone to absorb oxygen, we degassed it and prepared the solutions in N_2 atmosphere just prior to the measurements.

VUV absorption measurements were performed at the beamline 1B of the UVSOR facility in IMS, by using the light monochromatized by a 1 m Seya-Namioka monochromator. The resolution was estimated to be about 0.4 nm. We used a solution cell consisting of two LiF windows and a 100 μm thick spacer of tetrafluoroethylene film between them. The $C_{60}F_x$ solutions were injected into the cell in N_2 atmosphere. We measured the solutions of $C_{60}F_{36}$ with a unique x value and $C_{60}F_{42}$ (overall). The former was a saturated solution, and the latter included 15.1 mg of powder dissolved in 6 mL of solvent. The spectral energy range was limited below 7.3 eV, which is the onset energy of the absorption by the solvent.

XPS measurements were performed with ESCALAB 220i of VG Co. Ltd. by using the Mg Kα line of $h\nu = 1253.9$ eV. The fluorine content of the sample was obtained from the peak area ratio of the two C 1s peaks corresponding to the residual double-bond carbon and the fluorinated carbon. The energy calibration was carried out by referring to the $4f_{7/2}$ peak of Au (83.9 eV).[22] The resolution was estimated to be 1.0 eV by the fwhm of the Ag 3d peak.

We also performed the simulations of the UPS and electronic absorption spectra of $C_{60}F_{36}$ with semiempirical calculations. On the basis of theoretical analyses on $C_{60}H_{36}$, Attalla et al.,[14] Austin et al.,[15] and Dunlap et al.[16] have reported that the isomers with T_h, D_{3d} and S_6, and T symmetries are stable, respectively. Therefore, we performed simulations for four $C_{60}F_{36}$ isomers with these symmetries by the ZINDO method in the program package CAChe. The geometrical optimization of the molecules was carried out with AM1 calculations. For the UPS spectra, the densities of occupied states of $C_{60}F_{36}$ isomers were deduced by convoluting delta functions at each calculated molecular orbital energy with a Gaussian function of 0.5 eV fwhm. The ZINDO simulations of the electronic absorption spectra of $C_{60}F_{36}$ isomers were performed by CI calculations including 81 configurations obtained by exciting one electron from any of the nine highest occupied molecular orbitals into any of the nine lowest unoccupied molecular orbitals.

III. Results and Discussion

1. XPS. In Figure 1 we show the C 1s XPS spectra of C_{60} and $C_{60}F_{48}$ as a typical example of fluorinated fullerene. The XPS spectrum of C_{60} (a) shows only one C 1s peak at 284.7 eV relative to the Fermi level, corresponding to the fact that all the carbon atoms of C_{60} are equivalent. The XPS spectrum of $C_{60}F_{48}$ (b) has two peaks. The binding energy of the fluorinated carbons (288.4 eV) is higher than that of the unsubstituted

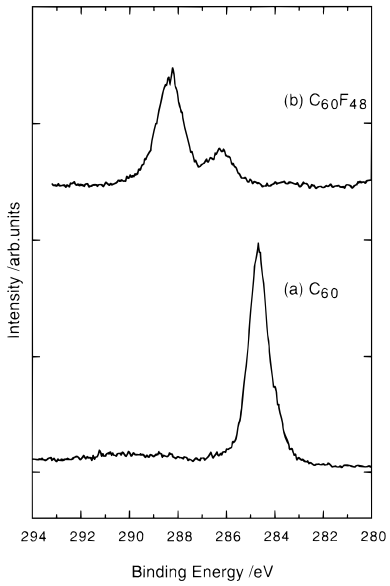

Figure 1. C 1s XPS spectra of C_{60} and $C_{60}F_{48}$ by the Mg Kα line.

double-bond carbons (286.2 eV). As described above, the fluorine content x of the fluorinated fullerene was determined from the ratio of the two peak areas.

2. NEXAFS. Figure 2a−c shows the C K-edge NEXAFS spectra of C_{60} and $C_{60}F_x$. The abscissa is the photon energy. The ordinate is the photoelectron yield which corresponds to the absorption intensity. Following the previous reports,[23] the sharp peaks in the low energy region and the broad structures in the higher energy region of the C_{60} spectrum (a) can be assigned to the transitions from the core levels to the π^* and the σ^* states, respectively. Fluorination brings about (1) intensity decrease of the low energy features and (2) intensity increase of the higher energy structures. The change of the spectral shape also indicates the change of the bonding state of carbons.

These changes can be interpreted that fluorine atoms are attached to the double bonds to modify the bonding states of carbons from sp^2 to sp^3, with the formation of C−F covalent bonds. As seen in Figure 2b,c, the degree of intensity change is parallel with the fluorine content. The decrease of the number of double bonds results in the reduction of the size of the π-conjugated system, leading to the decrease of the width of the π^* band. The disappearance of the high energy part of the π^* states of C_{60} spectrum should correspond to this change. Even in the spectrum of the highly fluorinated fullerene $C_{60}F_{40}$, however, we still see the lowest energy peak due to the transition to the π^* LUMO. This manifests that double bonds still exist. We also see that this peak remains at the same energy (284.1 eV) as that of the spectrum of C_{60}.

In Figure 2d we show the partial density of unoccupied states of $C_{60}F_{48}$ consisting of the C 2p orbitals, which we previously calculated by the DV-Xα method.[10] This simulated spectrum and the observed spectrum of $C_{60}F_{40}$ (c) show reasonably good correspondence in that the π^* and σ^* regions are well separated with an isolated low energy π^* peak.

In Figure 3, a and b, we show the F K-edge NEXAFS spectra of $C_{60}F_{22}$ and $C_{60}F_{40}$, respectively. They consist of (1) a broad peak at about 690 eV with a shoulder at the higher energy side and (2) a broad structure extending into the higher energy region. In Figure 3d we also show the spectrum of perfluorotetracosane (n-$C_{24}F_{50}$),[24] which is a typical molecule with covalent C−F bonds. The spectra of $C_{60}F_x$ and n-$C_{24}F_{50}$ show roughly similar spectral features except for a shift of about 5 eV, which may

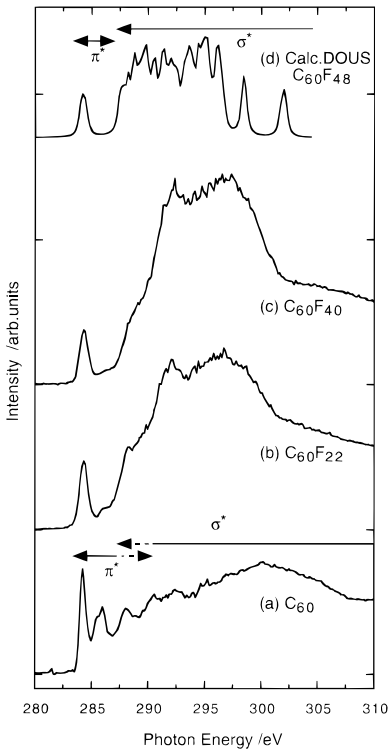

Figure 2. Observed and calculated C K-edge NEXAFS spectra of $C_{60}F_x$: (a) observed spectrum of C_{60}; (b, c) observed spectra of $C_{60}F_x$ with $x = 22$ (b) and $x = 40$ (c); and (d) calculated spectrum of $C_{60}F_{48}$ by DV-Xα method (ref 10).

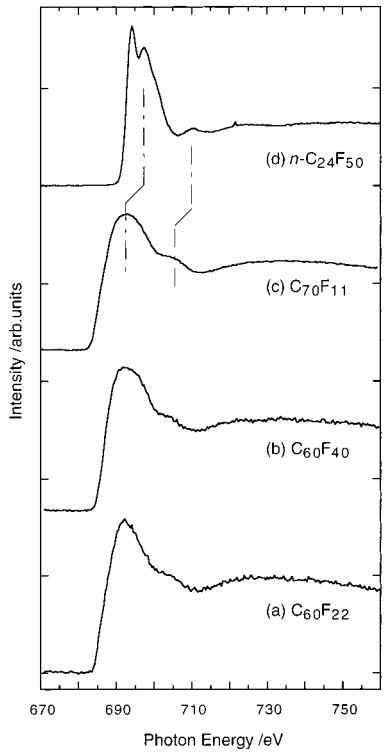

Figure 3. F K-edge NEXAFS spectra of $C_{60}F_{22}$ (a), $C_{60}F_{40}$ (b), and $C_{70}F_{11}$ (c) compared with the spectrum of perfluorotetracosane (n-$C_{24}F_{50}$) (d) (ref 24).

be ascribed to the difference of the F 1s ionization energy. This similarity is consistent with the C−F covalent bond formation by fluorination of C_{60}.

Figure 4 shows the C K-edge spectra of C_{70} and $C_{70}F_{11}$. As in the case of C_{60}, the spectrum of C_{70} shows sharp peaks in

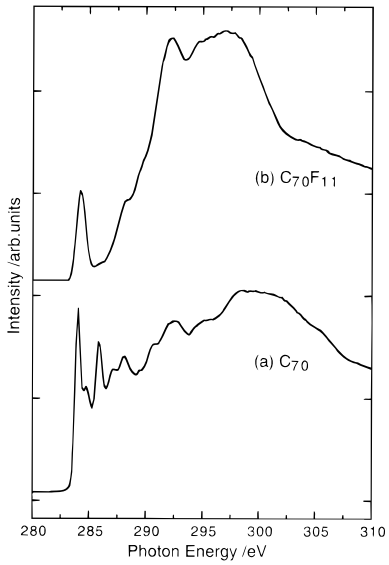

Figure 4. C K-edge NEXAFS spectra of C_{70} and $C_{70}F_{11}$.

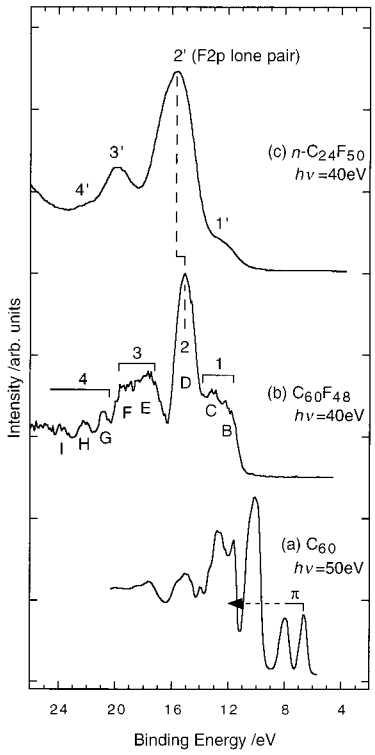

Figure 5. UV photoemssion spectrum of $C_{60}F_{48}$ (b) in comparison with those of C_{60} (a) (ref 25) and perfluorotetracosane (*n*-$C_{24}F_{50}$) (c) (ref 26).

the low energy region and a broad structure at the higher energy region, which are ascribed to the transitions to the π^* and σ^* states, respectively. On fluorination, the former becomes weaker, while the latter becomes stronger. These trends and the resultant spectrum are similar to those of $C_{60}F_x$. The F K-edge spectrum of $C_{70}F_{11}$ in Figure 3c also shows a structure similar to those of $C_{60}F_x$ and perfluorotetracosane. These changes indicate that the bonding state of the carbon in C_{70} also becomes sp^3 by fluorination, with the formation of C−F bonds.

3. UPS. Figure 5b shows the UPS spectrum of $C_{60}F_{48}$ at photon energy $h\nu = 40$ eV. The abscissa is the binding energy relative to the vacuum level. In Figure 5, a and c, we also show the spectra of C_{60}[25] and perfluorotetracosane (*n*-$C_{24}F_{50}$),[26] respectively. The spectrum of $C_{60}F_{48}$ (b) shows good agreement with the reported spectrum of $C_{60}F_{46\pm2}$,[5] except that our spectrum shows finer structures. This spectrum shows the following features: (1) the shoulders B and C at 12 and 13 eV, (2) the prominent peak D at 15 eV, (3) the broad structures E and F between 17 and 20 eV, and (4) the peaks and structures G−I in the higher binding energy region. The X-ray photoemission spectrum of $C_{60}F_{42}$ reported by Ibrahim et al.[27] shows corresponding structures, but they did not discuss the detail. Theoretical calculations described below indicate that the peak D is mostly derived from the 2p lone pairs of fluorine atoms. Due to their nonbonding nature, the lone pair orbitals have similar energy and form a strong peak.

The spectrum of *n*-$C_{24}F_{50}$ (Figure 5c) shows a generally good correspondence with the spectrum of $C_{60}F_{48}$ (b). According to the ab initio MO calculations on poly(tetrafluoroethylene) $(CF_2)_n$,[28] the features 1′−4′ of the spectrum of *n*-$C_{24}F_{50}$ (c) can be ascribed as follows: (2′) F 2p lone pairs; (4′) C 2s states, and the region spanning from 10 to 20 eV (1′ and 3′) corresponds to the levels derived from the interacting C 2p and F 2p orbitals. The sharp and intense peak 2′ at 15.6 eV of F 2p lone pair character corresponds to peak 2 for $C_{60}F_{48}$. The good correspondence between the spectra of $C_{60}F_{48}$ and *n*-$C_{24}F_{50}$ also suggests the similarity of the features 1−4 with 1′−4′, respectively. This point will be discussed further later.

The levels derived from the π orbitals span in the lower binding energy region <12 eV in the spectrum of C_{60} (a).[29] The lowest two peaks in this region were assigned to the degenerate pure π orbitals.[25] No feature corresponding to these peaks is seen in the present spectrum of $C_{60}F_{48}$ (b). This change by fluorination can be explained as follows: fluorine atoms are attached to the C_{60} cage, and part of the double bonds are broken; then the remaining double bonds become less conjugated, leading to the decrease of the width of the π levels.

On the other hand, the results of NEXAFS measurements described above clearly indicate that some π^* states still remain even after heavy fluorination. To examine their contribution to the UPS spectra, we closely examined the right-hand onset region of the UPS spectra of fluorinated C_{60} by using low energy light sources. Figure 6 shows the spectra of heavily doped $C_{60}F_{48}$ at various photon energies. The He I ($h\nu = 21.2$ eV) spectrum (b) is similar to that at $h\nu = 40$ eV (a) but also shows a faint structure (hatched) around 10 eV, indicating that the true threshold is at lower energy than 10 eV. The Ar I ($h\nu = 11.7$ eV) spectrum (c) more clearly shows this feature with the ionization threshold energy I_{th} at 8.4 eV. This structure, indicating the contribution from the highest occupied molecular orbitals of these fluorinated fullerenes, is probably due to the π orbitals derived from double bonds remaining after fluorination. We also note that this I_{th} of 8.4 eV is still significantly higher than the value of $I_{th} = 6.2$ eV of C_{60}, reflecting the reduction of the size of the π-conjugated system.

We expect that this feature in the low binding energy region will be stronger in the spectra of less fluorinated C_{60}. Figure 7b−e shows the UPS spectra of $C_{60}F_{30}$ and $C_{60}F_{36}$ compared with those of C_{60} (a) and $C_{60}F_{48}$ (f). At first, we examine the He I spectra at $h\nu = 21.2$ eV. The He I spectra of $C_{60}F_{30}$ (b) and $C_{60}F_{36}$ (d) already show the clear peak D at 15 eV as in the spectrum of $C_{60}F_{48}$ (f). We note that the intensity ratio of the peak D to the shoulders B and C at 12−13 eV increases with increasing fluorine content, consistent with the assignment of the peak to the F 2p lone pairs.

The spectra of the lightly doped C_{60} differ from that of heavily doped C_{60} (f) in the threshold region on the right-hand side of

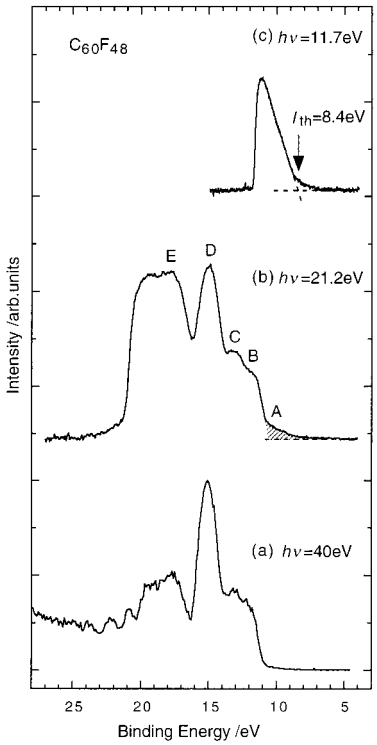

Figure 6. UV photoemission spectra of $C_{60}F_{48}$ at various photon energies: (a) $h\nu = 40$ eV, (b) He I line ($h\nu = 21.2$ eV), and (c) Ar I line ($h\nu = 11.7$ eV).

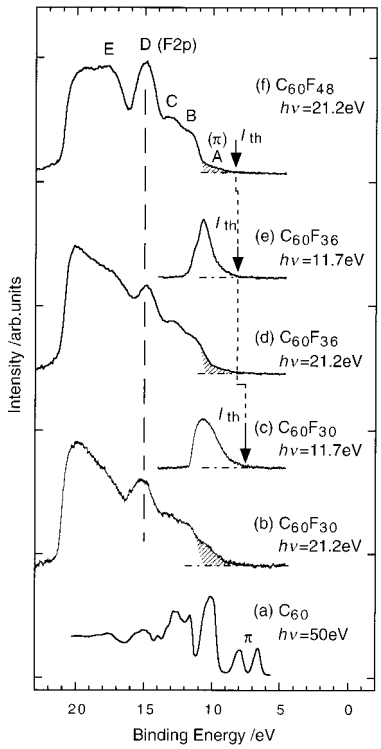

Figure 7. UV photoemssion spectra of lightly doped $C_{60}F_x$ (b−e) compared with those of C_{60} (a) (ref 25) and $C_{60}F_{48}$ (f). The arrows point to the onsets of the spectra corresponding to the ionization threshold energy I_{th}.

the spectra. As the fluorine content increases, the hatched structure A in the region of binding energy <11 eV loses its intensity, and its onset shifts to higher binding energy.

The work functions of $C_{60}F_{30}$, $C_{60}F_{36}$, and $C_{60}F_{48}$ were 5.6, 5.2, and 5.4 eV, respectively, while the ionization threshold energies I_{th} obtained from the Ar I spectra of $C_{60}F_{30}$ and $C_{60}F_{36}$ (Figure 7c,e) were 7.6 and 8.2 eV, respectively. This increase of I_{th} with x is consistent with the progress of the breaking of the π-delocalized systems with fluorination. Thus, the UPS spectra by the low-$h\nu$ resonance lines have clearly revealed the existence of the spectral feature A in the low binding energy region and the dependence of its intensity and onset energy on the degree of fluorination. For $C_{60}F_x$ with $x > 30$, the residual double bonds will be mostly isolated by single bonds. This may be the reason for the lack of drastic change of the spectra, except for the change in the relative intensity described above.

In Figure 8b,c, we show the UPS spectra of $C_{70}F_{45}$ obtained with the He I and Ar I resonance lines. The He I spectrum (b) shows spectral features similar to that of $C_{60}F_x$. We also show the spectrum (a) of C_{70} at $h\nu = 45$ eV by Jost et al.[30] as a reference. We see that fluorination of C_{70} brings about changes similar to that in the case of $C_{60}F_x$. From the Ar I spectrum (c) we obtain the threshold ionization energy to be 7.8 eV, which is similar to that of $C_{60}F_{30}$ (7.6 eV). This suggests that the π-conjugated system of $C_{70}F_{45}$ has a dimension similar to that of $C_{60}F_{30}$.

Now we will examine the UPS spectra by using simulated spectra. For $C_{60}F_{48}$, attempts to reproduce the density of states by the local density functional approximation[5] and the DV-Xα method[10] have been reported. They both reproduced the structures in the higher energy region, but they show almost no level in the lower energy region than the F 2p peak, in sharp contradiction to the experimental results.

In Figure 9, we show the observed spectrum of $C_{60}F_{36}$ (a) and the presently simulated density of occupied states (b)−(e)

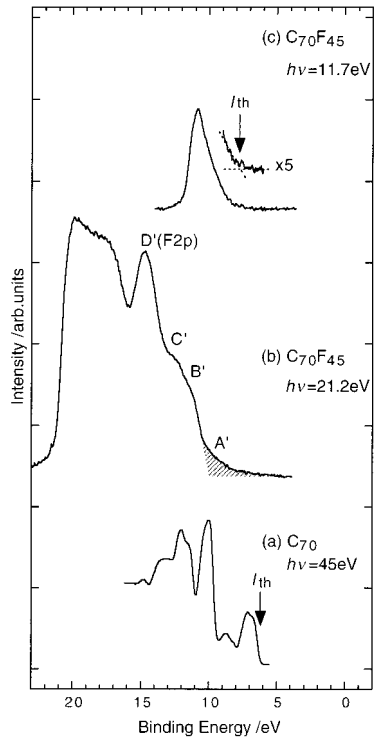

Figure 8. UV photoemssion spectra of $C_{70}F_{45}$ (b, c) in comparison with that of C_{70} (a) (ref 30).

by the ZINDO method for the $C_{60}F_{36}$ isomers with T_h, D_{3d}, S_6, and T symmetries. In Table 1 we show the relative values of heat of formation: $\Delta_f H$'s obtained by the AM1 optimization to that of the isomer of T symmetry for these $C_{60}F_{36}$ isomers. All the calculations of $C_{60}F_{36}$ for the four isomers gave a sharp peak at about 15 eV and structures in the lower energy region. They correspond to the peak D and the structures A−C of the

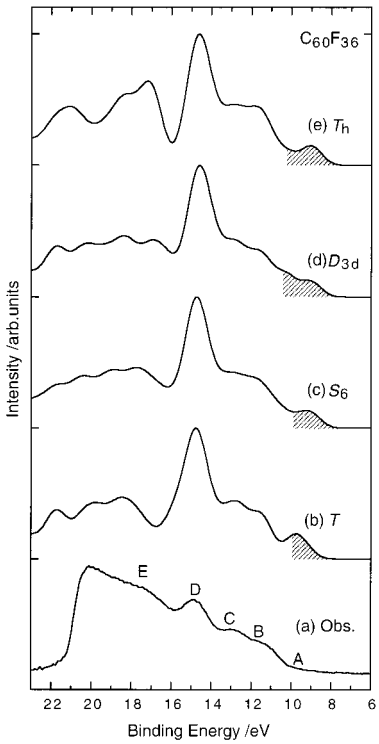

Figure 9. Observed and simulated UV photoemission spectra of $C_{60}F_{36}$.

TABLE 1: $\Delta_f H$'s of the $C_{60}F_{36}$ Isomers

symmetry	relative energy/eV
D_{3d}	3.74
T_h	2.43
S_6	1.54
T	0.00

observed spectrum (a). According to the wave functions in the calculations, the sharp peak originates mostly from fluorine 2p orbitals, and the lower binding energy structures corresponding to structure A in the observed spectrum originate mostly from the orbitals of carbons in all the simulated spectra. Especially, the hatched region shows the range of the molecular orbitals consisting of only π orbitals of the residual double-bond carbons. These results support the interpretations described above that structure A is due to the π orbitals derived from the double bonds and also consistent with the assignments of the UV photoemission spectrum of *n*-$C_{24}F_{50}$ in Figure 5c. We are unable to suggest the symmetry of $C_{60}F_{36}$ from the present comparison, since the differences among the simulated spectra (b)−(e) are not so significant. If the measurements in better resolution and with better isomer-separated specimen give spectra with finer structures, certain information about the symmetry may be obtained.

4. Vacuum-UV Absorption. In Figure 10, b and c, we show the vacuum-UV absorption spectra of $C_{60}F_{36}$ (unique *x*) and $C_{60}F_{42}$, respectively. They have a broad structure peaked at 6.5 and 6.7 eV, respectively, with a faint shoulder at the lower energy side. These two spectra resemble each other, indicating that their HOMO−LUMO gaps are almost the same. While the electronic absorption spectrum of C_{60} (a) reported by Ajie[31] shows several peaks, the presently observed spectra have no sharp peaks in the UV−visible region, indicating that fluorination decreased the number of double bonds, and the degree of conjugation of the fullerene was lowered. The spectra of poly(tetrafluoroethylene) $(CF_2)_n$[32] and poly(1,3-hexafluorobutadiene) $(C(CF_3)=C(CF_3))_n$[33] have absorption peaks at 7.6 and 6.7 eV, respectively. The double bonds in the latter case are expected

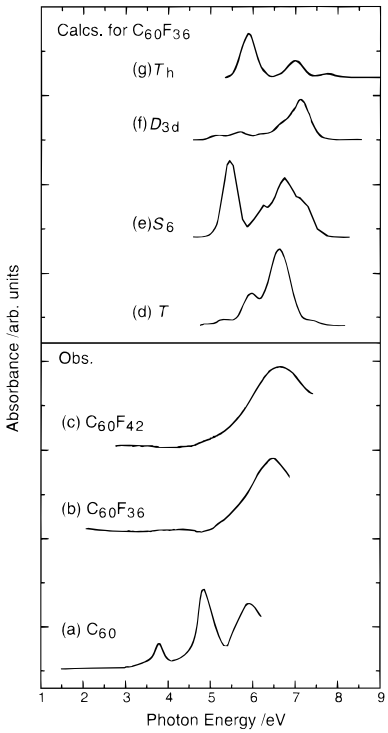

Figure 10. Observed and simulated electronic absorption spectra of $C_{60}F_x$. The lower panel shows the observed electronic spectra of $C_{60}F_x$ (b, c) in perfluoromethylcyclohexane and the reported electronic spectrum of C_{60} (a) (ref 31), and the upper panel shows the calculated spectra for four geometrical isomers of the $C_{60}F_{36}$ molecule by the ZINDO method.

not to be conjugated due to the steric hindrance. The latter value is similar to those of $C_{60}F_x$, both corresponding to the absorption in a fairly localized double bond in heavily fluorinated systems.

In Figure 10d−g, we also show the theoretically simulated absorption spectra of $C_{60}F_{36}$ by ZINDO calculations. These simulations were performed for the same isomers as in the simulations of the density of occupied states in the preceding section. Each simulated spectrum has characteristic features. If the observed spectrum agrees with one of the calculated spectra, we can identify the symmetry of the $C_{60}F_x$ molecule used in the present study. Unfortunately, however, the observed spectra are much broader than the calculated spectra, and no clear identification can be made at present. Still we see that the correspondence with T and D_{3d} isomers is better than S_6 and T_h isomers in that absorption in the higher energy region.

We can consider two probable reasons for broadening of the observed spectra. One is that the fluorine number of the sample is not unique but has some distribution. Another is that the sample is mixture of geometrical isomers. As for $C_{60}F_{36}$, the former factor can be eliminated because mass spectrometry showed only 36 as the mass number. The reported ^{19}F NMR measurements[13] indicated that $C_{60}F_{36}$ has several symmetries. Thus, it seems necessary to separate $C_{60}F_x$ with a single number of fluorines further into geometrical isomers for more detailed study of the absorption spectra.

5. Discussion of the Electronic Structures of C_{60} and $C_{60}F_x$. On the basis of the present measurements and literature, we can compose the energy diagrams of $C_{60}F_x$ and C_{60} shown in Figure 11. Each diagram consists of C 1s core, LUMO, HOMO, and Fermi levels and covers the vapor and solid phases. The origin of the energy axis is the vacuum level.

The left half of Figure 11 summarizes the information about C_{60}. The ionization threshold energy I_{th} (the HOMO energy)

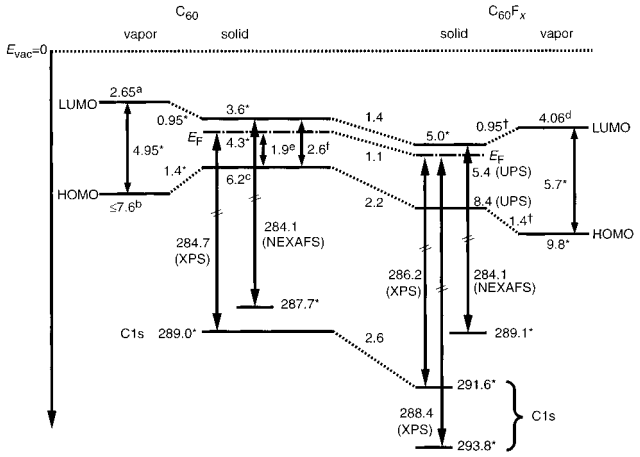

Figure 11. Energy diagrams of C_{60} and $C_{60}F_x$ relative to the vacuum level: (a) ref 35, (b) ref 34, (c) ref 36, (d) ref 6, (e) ref 37, (f) ref 38. †Assumed to be same as the corresponding quantity of C_{60}. *Derived from the experimental values, the reported values, and the values with †.

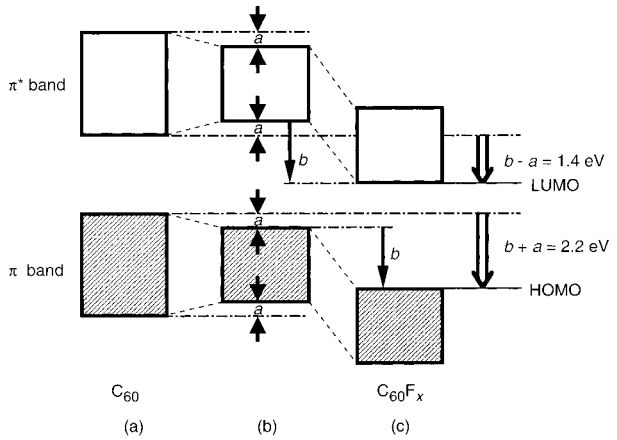

Figure 12. Schematic energy diagram for the influences of fluorination upon the π and π^* bands of C_{60}. (a) The π and π^* bands of C_{60}. (b) The reduction of the π conjugation leads to the narrowing of $2a$ of the π and π^* bandwidth. At the same time, (c) the inductive effect lowers the two bands by b.

and the electron affinity (the LUMO energy) for the vapor phase were taken from the literature.[34,35] For solid C_{60}, UPS measurements by Sato et al.[36] gave 6.2 eV as the ionization threshold energy I_{th}. Takahashi et al.[37] reported $I_{th} = 1.9$ eV relative to the Fermi level E_F. Benning et al.[38] reported the HOMO−LUMO separation to be 2.6 eV from UPS and IPES measurements. From these reports, we could obtain the energies of the LUMO, the Fermi level, and the HOMO of solid C_{60} to be 3.6, 4.3, and 6.2 eV, respectively. We note that the energies of the LUMO and the HOMO are shifted in going from the vapor to the solid phases by 0.95 and 1.4 eV, respectively, due to the polarization of the surrounding molecules.[39] The energy of the C 1s core level was estimated to be 284.7 eV relative to the Fermi level in the present XPS measurements. This value can be converted to a value of 289.0 eV relative to the vacuum level.

On the right half of Figure 11, we summarized the corresponding values of $C_{60}F_x$ in the vapor and solid phases. The data are for the heavily doped $C_{60}F_x$ with x over 40, for which extensive information is available. Jin et al.[6] measured the electron affinity of the $C_{60}F_{48}$ molecule to be 4.06 eV. Our UPS present measurements gave 5.4 and 8.4 eV as the energies of the Fermi and the HOMO levels of solid $C_{60}F_{48}$, respectively. Since we have no experimental data about the polarization energy for an electron in $C_{60}F_x$, we assumed it to be the same as the value for C_{60} (0.95 eV). This leads to the LUMO energy of $C_{60}F_x$ of 5.0 eV. As for the HOMO level of vapor $C_{60}F_x$, a similar assumption of the same polarization energy for a hole in $C_{60}F_x$ as that of C_{60} gives the HOMO energy of 9.8 eV. The lower energy peak in the XPS spectrum of $C_{60}F_x$ corresponds to the remaining double-bond carbons, and its binding energy of 286.2 eV relative to the Fermi level is converted to 291.6 eV relative to the vacuum level. Similarly, the binding energy of the fluorinated carbons can be deduced to be 293.8 eV relative to the vacuum level.

Next we discuss the change of the electronic structure of C_{60} by fluorination. In Figure 11, we see all the energy levels of $C_{60}F_x$ become stabilized from the corresponding levels of C_{60}. This change can be ascribed to the strong inductive effect of electronegative fluorine atoms. We also see that the HOMO and the LUMO levels of C_{60} are lowered by different amounts of 2.2 and 1.4 eV, respectively.

This difference can be explained by taking account of the change of the π-conjugation in addition to the inductive effect. In Figure 12, we show the influences by these two effects. The fluorination changes the double bonds of the fullerene into single bonds. The residual double bonds become isolated, and the size of the π-conjugated system on the C_{60} cage becomes reduced. The reduction of the π-conjugation leads to the narrowing of the π and π^* bands as shown in Figure 12b. At the same time, the inductive effect lowers the two bands as shown in Figure 12c. We can estimate the results of these two effects by assuming a common magnitude of the narrowing of the π and π^* bandwidths of $2a$ and the lowering by the inductive effect of b. As for the HOMO, the two effects work concertedly to make the HOMO deeper by $b + a$ (=2.2 eV). As for the LUMO, on the other hand, the two effects work in opposite directions. The inductive effect lowers the LUMO, while the narrowing of the π^* bandwidth raises the LUMO. As a combined effect, the inductive effect dominates and leads to the lowering of the LUMO by $b - a$ (=1.4 eV). From these relations, we find $a = 0.4$ eV and $b = 1.8$ eV, respectively. Thus, we could quantitatively explain how these two effects influence the HOMO and the LUMO levels in different ways.

The Fermi level is also lowered by 1.1 eV after fluorination in Figure 11. Usually the work functions of organic materials are in the range between 4.1 and 5.0 eV.[40] The work function of $C_{60}F_x$ (5.6, 5.2, and 5.4 eV for $x = 30$, 36, and 48, respectively) observed in the present measurements is considerably larger than these results. This suggests that $C_{60}F_x$ is a very strong electron acceptor.

From the estimated energies of the HOMO and LUMO of the $C_{60}F_x$ molecule in the gas phase, we can estimate the HOMO−LUMO gap to be 5.7 eV. This corresponds to the absorption tail in the observed VUV absorption spectra in Figure 10.

From the XPS measurements, we can estimate the C 1s binding energy relative to the vacuum level. The value for the carbon atoms in the double bonds of $C_{60}F_x$ is 2.6 eV higher than that of C_{60}. This change can be ascribed to the inductive effect of fluorine. On the other hand, the NEXAFS measurements in Figure 2 gave the same transition energy of 284.1 eV from the C 1s levels of double-bond carbons to the LUMO for both C_{60} and $C_{60}F_x$. When we simply estimate the transition energy from the C 1s level of the double-bond carbons to the LUMO by using the XPS C 1s peak energies, the transition energies are obtained to be 285.4 and 286.6 eV for C_{60} and $C_{60}F_x$, respectively. These estimated energies are larger than

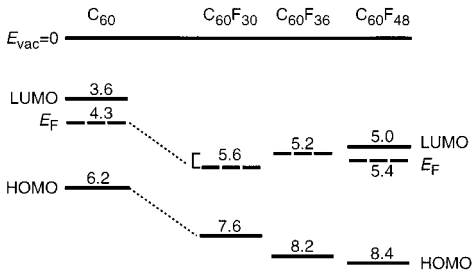

Figure 13. Change of the energy of the Fermi and the HOMO levels of $C_{60}F_x$ with x.

those by NEXAFS measurements by 1.3 and 2.5 eV, respectively. These deviations correspond to the binding energies of core exciton, which is the pair of the excited electron and the core hole.

We have already reported[41] that such an excitonic effect is correlated with the dimension of the π-conjugated system. When the effective size of the π-conjugated system surrounding the excited atom is large, the effect of the core hole on π^* orbitals becomes reduced due to the screening by the delocalized π electrons. Thus, the larger excitonic effect in $C_{60}F_x$ than in C_{60} may reflect the less effective screening due to the reduction of the π-conjugated system by fluorination.

In Figure 13, we show how the energies of the Fermi and the HOMO levels obtained in UPS measurements change depending on the degree of fluorination. We see that the ionization threshold energy gradually increases with fluorination. This change is consistent with the interpretation that fluorination makes the HOMO level deeper. On the other hand, the Fermi energies show no simple correlation with the degree of fluorination. This may be caused by the presence of mixed geometrical isomers in $C_{60}F_x$ with intermediate values of x. The different isomers will have various distributions of double bonds over the molecule, which will lead to different electronic structures. More studies are required to examine the effect of such isomerism of $C_{60}F_x$.

IV. Conclusion

We investigated the chemical bonding and the electronic structures of $C_{60}F_x$ and $C_{70}F_x$, by using NEXAFS, UV photoemission, and X-ray photoelectron spectroscopies. As fluorination proceeds, the electronic structure of the fullerenes gradually changes due to the formation of C−F bonds accompanied by the change of the bonding state of carbon atoms from sp^2 to sp^3. We derived an energy diagram of heavily fluorinated $C_{60}F_x$ and explained the change of the electronic structure with the combination of the reduction of π and π^* bandwidths and the inductive effect by the electronegative fluorine atoms. The vacuum-UV absorption spectra of $C_{60}F_x$ solutions were also measured and compared with the simulated spectra of geometrical isomers. For $C_{60}F_x$ with $x > 30$, the electronic structures of $C_{60}F_x$ do not show a drastic dependence on x, probably because the residual double bonds of the fullerene cage surface are almost isolated. These results, together with the theoretical calculations, gave a basic understanding of the electronic structure of these materials and also showed unique aspects of the electronic structure such as the large electron affinity and the work function. For further clarification of the electronic structures of fluorinated fullerenes, the preparation and the measurements of isomer-separated specimens are highly desired.

Note Added in Proof. After completion of this work, we found a paper reporting ionization energies of highly fluorinated C_{60} and C_{70} (Steger et al., *Chem. Phys. Lett.* **1997**, *276*, 39). They reported the ionization energy of 12.0 eV for $C_{60}F_{46,48}$ in the gas phase. Our result for solid $C_{60}F_{48}$ is 8.4 eV. When we assume the polarization energy for a hole of solid $C_{60}F_{48}$ to be same as the value of C_{60} (1.4 eV), the HOMO energy of molecular $C_{60}F_{48}$ is 9.8 eV. This value is much different from the value reported by Steger et al. The origin of the difference is not clear at present.

Acknowledgment. We are grateful to Prof. A. Yagishita, Dr. Y. Kitajima, and Dr. S. Tanaka for the kind help with the NEXAFS studies, to Dr. S. Hasegawa and Mr. K. Sugiyama for the help with UPS studies, and to Mr. M. Hasumoto for the help with the vacuum-UV absorption studies. We are also thankful to Mr. K. Suzuki at the Instrument Department Center of School of Science at Nagoya University for the construction of the VUV solution cell. This work was carried out under the approval of the Program committee of Photon Factory (Nos. 93-G324 and 95-G374) and as the Joint Studies Program of UVSOR (No. 6-H217). It was supported in part by the Grants in Aid for Scientific Research (Nos. 07213216, 07NP0303, 07CE2004, and 08640643) from the Ministry of Education, Science and Culture of Japan and by the Venture Business Laboratory Program "Advanced Nanoprocess Technologies" of Nagoya University.

References and Notes

(1) Kroto, H. W.; Heath, J. R.; O'Brien, S. C.; Curl, R. F.; Smalley, R. E. *Nature (London)* **1985**, *318*, 162.
(2) Touhara, H.; Okino, F.; Yajima, S.; Suganuma, S.; Seki, K.; Mitsumoto, R.; Fujimoto, F. *Trans. Mater. Res. Soc. Jpn.* **1994**, *14B*, 1173.
(3) Okino, F.; Yajima, S.; Suganuma, S.; Mitsumoto, R.; Seki, K.; Touhara, H. *Synth. Met.* **1995**, *70*, 1447.
(4) Liu, N.; Touhara, H.; Okino, F.; Kawasaki, S.; Nakacho, Y. *J. Electrochem. Soc.* **1996**, *143*, 2267.
(5) Benning, P. J.; Ohno, T. R.; Weaver, J. H.; Mukherjee, P.; Adcock, J. L.; Compton, R. N.; Dunlap, B. I. *Phys. Rev. B* **1993**, *47*, 1589.
(6) Jin, C.; Hettich, R. L.; Compton, R. N.; Tuinman, A.; Derecskei-Kovacs, A.; Marynics, D. S.; Dunlap, B. I. *Phys. Rev. Lett.* **1994**, *73*, 2821.
(7) Kniaz, K.; Fischer, J. E.; Selig, H.; Vaughan, G. B. M.; Romanov, W. J.; Cox, D. M.; Chowdhury, S. K.; McCauley, J. P.; Strogin, R. M.; Smith, A. B., III. *J. Am. Chem. Soc.* **1993**, *115*, 6060.
(8) Tuinman, A. A.; Mukherjee, P.; Adcock, J. L.; Hettich, R. L.; Compton, R. L. *J. Phys. Chem.* **1992**, *96*, 7584.
(9) Cox, D. M.; Cameron, S. D.; Tuinman, A.; Gakh, A.; Adocock, J. L.; Compton, R. N.; Hagaman, E. W.; Kniaz, K.; Fischer, J. E.; Strongin, R. M.; Cichy, M. A.; Smith, A. B., III. *J. Am. Chem. Soc.* **1994**, *116*, 1115.
(10) Kawasaki, S.; Okino F.; Touhara, H.; Sonoda, T. *Phys. Rev. B* **1996**, *53*, 16652.
(11) Okino, F.; Touhara, H.; Seki, K.; Mitsumoto, R.; Shigematsu, K.; Achiba, Y. *Fullerene Sci. Technol.* **1993**, *1* (3), 425.
(12) Gakh, A. A.; Tuinman, A. A.; Adcock, J. L.; Sachleben, R. A.; Compton, R. N. *J. Am. Chem. Soc.* **1994**, *116*, 819.
(13) Boltalina, O. V.; Bolshevskii, A. Y.; Sidorov, L. N.; Street, J. M.; Taylor, R. *J Chem. Soc., Chem. Commun.* **1996**, 529.
(14) Attalla, M. I.; Vassallo, A. M.; Tattam, B. N.; Hanna, J. V. *J. Phys. Chem.* **1993**, *97*, 6329.
(15) Austin, S. J.; Batten, R. C.; Fowler, P. W.; Redmond, D. B.; Tayor, R. *J. Chem. Soc., Perkin Trans.* **1993**, *2*, 1383.
(16) Dunlap, B. I.; Brenner, D. W.; Schriver, G. W. *J. Phys. Chem.* **1994**, *98*, 1756.
(17) Stöhr, J. *NEXAFS Spectroscopy*; Springer: Berlin, 1992.
(18) Kikuchi, K.; Nakahara, N.; Wakabayashi, T.; Honda, M.; Matsumiya, H.; Moriwaki, T.; Suzuki, S.; Shiromaru, H.; Saito, K.; Yamauchi, K.; Ikemoto, I.; Achiba, Y. *Chem. Phys. Lett.* **1992**, *188*, 177.
(19) Narioka, S.; Ishii, H.; Ouchi, Y.; Yokoyama, T.; Ohta, T.; Seki, K. *J. Phys. Chem.* **1995**, *99*, 1332.
(20) Stöhr, J.; Jaeger, R. *Phys. Rev. B* **1982**, *26*, 4111.
(21) Seki, K.; Nakagawa, H.; Fukui, K.; Ishiguro, E.; Kato, R.; Mori, T.; Sakai, K.; Watanabe, M. *Nucl. Instrum. Methods A* **1986**, *246*, 264.
(22) Fuggle, J. C.; Mårtensson, N. *J. Electron Spectrosc. Relat. Phenom.* **1980**, *21*, 275.

(23) Terminello, L. J.; Shuh, D. K.; Himpsel, F. J.; Lapiano-Smith, D. A.; Stöhr, J.; Bethune, D. S.; Meijer, G. *Chem. Phys. Lett.* **1991**, *182*, 492.
(24) Nagayama, K.; Mitsumoto, R.; Araki, T.; Ouchi, Y.; Seki, K. *Physica B* **1995**, *208*, 419.
(25) Weaver, J. H.; Martins, J. L.; Komeda, T.; Chen, Y.; Ohno, T. R.; Kroll, G. H.; Troullier, N.; Haufler, R. E.; Smalley, R. E. *Phys. Rev. B* **1991**, *66*, 1741.
(26) Miyamae, T., unpublished result.
(27) Ibrahim, K.; Liu, F. Q.; Jia, J. F.; Dong, Y. H.; Yang, Y.; Qian, H. J.; Lu, S. H.; Wu, S. C.; Gu, Z. N. *J. Electron Spectrosc. Relat. Phenom.* **1996**, *78*, 437.
(28) Seki, K.; Tnanaka, H.; Ohta, T.; Aoki, Y.; Imamura, Y.; Fujimoto, H.; Yamamoto, H.; Inokuchi, H. *Phys. Scr.* **1990**, *41*, 167.
(29) Martins, J. L.; Troullier, N.; Weaver, J. H. *Chem. Phys. Lett.* **1991**, *180*, 457.
(30) Jost, M. B.; Benning, P. J.; Poirier, D. M.; Weaver, J. H.; Chibante, L. P. F.; Smalley, R. E. *Chem. Phys. Lett.* **1991**, *184*, 423.
(31) Ajie, H.; Alvarez, M. M.; Anz, S. J.; Beck, R. D.; Diederich, F.; Fostiropoulos, K.; Huffman, D. R.; Krätchmer, W.; Rubin, Y.; Schriver, K. E.; Sensharma, D.; Whetten, R. L. *J. Phys. Chem.* **1990**, *94*, 8630.
(32) Nagayama, K.; Miyamae, T.; Mitsumoto, R.; Ishii, H.; Ouchi, Y.; Seki, K. *J. Electron Spectrosc. Relat. Phenom.* **1996**, *78*, 407.
(33) Mitsumoto, R.; Nishimura, S., unpublished results.
(34) Lichtenberger, D. L.; Nebsby, K. L.; Ray, C. D.; Huffman, D. R.; Lamb, L. D. *Chem. Phys. Lett.* **1991**, *176*, 203.
(35) Yang, S. H.; Petiette, C. L.; Conceicao, J.; Cheshnovsky, O.; Smalley, R. E. *Chem. Phys. Lett.* **1987**, *139*, 233.
(36) Sato, N.; Saito, Y.; Shinohara, H. *Chem. Phys.* **1992**, *162*, 433.
(37) Takahashi, T.; Morikawa, T.; Sato, S.; Katayama-Yoshida, H.; Yuyama, A.; Seki, K.; Fujimoto, H.; Hino, S.; Hasegawa, S.; Kamiya, K.; Inokuhci, H.; Kikuchi, K.; Suzuki, S.; Ikemoto, K.; Achiba, Y. *Physica C* **1991**, *185*, 417.
(38) Benning, P. J.; Poirier, D. M.; Ohno, T. R.; Chen, Y.; Jost, M. B.; Stepniak, F.; Kroll, G. H.; Weaver, J. H.; Fure, J.; Smalley, R. E. *Phys. Rev. B* **1992**, *45*, 6899.
(39) Wright, J. D. *Molecular Crystals*; Cambridge University: Cambridge, 1987.
(40) Kotani, M.; Akamatu, H. *Discuss. Faraday Soc.* **1971**, *51*, 94.
(41) Seki, K.; Mitsumoto, R.; Araki, T.; Ito, E.; Ouchi, Y.; Kikuchi, K.; Achiba, Y. *Synth. Met.* **1994**, *64*, 353.